

Running head: SYSTEM FOR RESEARCHING THE PUPIL LIGHT REFLEX

1

1

2

3

4 *PyPlr*: A versatile, integrated system of hardware and software for researching the human pupillary

5 light reflex

6

7 Joel T. Martin¹, Joana Pinto¹, Daniel Bulte¹, and Manuel Spitschan²

8

9 ¹Institute of Biomedical Engineering, Department of Engineering Science, University of Oxford,

10 United Kingdom, OX3 7DQ

11 ²Department of Experimental Psychology, University of Oxford, United Kingdom, OX2 6GG

12

13

14

Author Note

15 Address: Joel T. Martin, Institute of Biomedical Engineering, Department of Engineering Science,

16 University of Oxford, United Kingdom, OX3 7DQ

17 Phone: +44 (0) 1865 617687

18 Email: joel.t.martin36@gmail.com, joel.martin@eng.ox.ac.uk

19 The research was supported by funding from the Engineering and Physical Sciences Research Council

20 (EPSRC: EP/S021507/1), the Wellcome Trust (204686/Z/16/Z) and John Fell OUP Research Fund,

21 University of Oxford (0005460).

SYSTEM FOR RESEARCHING THE PUPIL LIGHT REFLEX

2

22 Abstract

23 We introduce *PyPlr*—a versatile, integrated system of hardware and software to support a broad
24 spectrum of research applications concerning the human pupillary light reflex (PLR). *PyPlr* is a
25 custom Python library for integrating a research-grade video-based eye-tracker system with a light
26 source and for streamlining stimulus design, optimisation and delivery, device synchronisation, and
27 extraction, cleaning, and analysis of pupil data. We additionally describe how full-field, homogenous
28 stimulation of the retina can be realised with a low-cost integrating sphere that serves as an alternative
29 to a more-complex Maxwellian view setup. Users can integrate their own light source, but we provide
30 full native software support for a high-end, commercial research-grade 10-primary light engine which
31 offers advanced control over the temporal and spectral properties of light stimuli as well as spectral
32 calibration utilities. Here, we describe the hardware and software in detail and demonstrate its
33 capabilities with two example applications: 1) pupillometer-style measurement and parametrisation of
34 the PLR to flash of white light, and 2) comparing the post-illumination pupil response (PIPR) to
35 flashes of long and short-wavelength light. The system holds promise for researchers who would
36 favour a flexible approach to studying the PLR and the ability to employ a wide range of temporally
37 and spectrally varying stimuli, including simple narrowband stimuli.

38 *Keywords:* pupillometry, instrumentation, pupillary light reflex, software, open source,
39 ganzfeld, melanopsin

SYSTEM FOR RESEARCHING THE PUPIL LIGHT REFLEX

3

40 *PyPlr*: A versatile, integrated system of hardware and software for researching the human pupillary
41 light reflex

42 **Introduction**

43 The pupillary light reflex (PLR) is the intrinsic mechanism of the pupil to constrict in
44 response to changing light levels. Though its precise biological purpose is still unclear, the PLR is
45 thought to optimise retinal image quality by regulating the amount of light that strikes the retina
46 (Hirata et al., 2003; McDougal & Gamlin, 2015), and it may also help to protect photoreceptors from
47 dangerous levels of light (Laughlin, 1992; Woodhouse & Campbell, 1975). Importantly, as the PLR
48 can be observed directly, it serves as a valuable tool for gaining insight into the integrity and activity
49 of the autonomic nervous system (Girkin, 2003). Indeed, subjective visual assessments of the PLR,
50 such as the swinging flashlight test (Levatin, 1959; Thompson, 1966), are still used routinely in
51 clinical investigations to unmask afferent pupillary defects and to give clues to a patient's
52 neurological state. Though useful in critical care, such techniques are less suited to research due to
53 their limited sensitivity and specificity, and to the poor inter and intraobserver reliability that exists
54 even among specialists (Litvan et al., 2000; Meeker et al., 2005). The advent and commercial
55 availability of video-based pupillometric techniques in the 1970s enabled researchers and clinical
56 practitioners to make repeatable and precise quantitative pupil measurements. As a consequence,
57 pupil's response to light is now well characterised in both health and disease (Loewenfeld, 1993).

58 The aperture of the pupil at any given time depends on the tone of the *dilator* and *sphincter*
59 *pupillae*—the two opponent smooth muscles of the iris. The iris sphincter receives parasympathetic
60 innervation and is almost solely responsible for the constriction of the pupil that follows an increase in
61 retinal illumination (McDougal & Gamlin, 2015). When light strikes the retina, photons are absorbed
62 by photoreceptors and the neural signal traverses a short reflex arc comprising the photoreceptor,
63 bipolar and ganglion cells of the retina (as well as other interneurons), the olivary pretectal nucleus of
64 the midbrain and the Edinger-Westphal nucleus, which projects to the iris sphincter muscle via the
65 ciliary ganglion (Hall & Chilcott, 2018). Following a sudden flash of white light, a normal pupil will
66 begin to constrict after approximately 230 ms and, after reaching peak constriction, will enter a
67 redilation phase and return to baseline. Redilation of the pupil upon light cessation depends on two

SYSTEM FOR RESEARCHING THE PUPIL LIGHT REFLEX

4

68 integrated processes: relaxation of the sphincter muscle due to parasympathetic inhibition, and
69 contraction of the dilator muscle following excitation in the sympathetic pathway (Szabadi, 2018).
70 The PLR is typically parametrised in terms of the latency, amplitude, velocity and acceleration of
71 change in pupil size and its dynamics are affected by normal ageing (Bitsios et al., 1996; Winston et
72 al., 2019). In a broad range of ophthalmic, neurological, and psychiatric conditions (Chen et al., 2011;
73 Girkin, 2003; Van Stavern et al., 2019), the PLR can be abnormal, making it an important tool in
74 research and diagnostics (Hall & Chilcott, 2018; Troiani, 2020).

75 Where it was once assumed that the PLR is controlled entirely by the integration of signals
76 from rod and cone photoreceptors, we now know that steady-state pupil size is largely under the
77 influence of intrinsically photosensitive retinal ganglion cells (ipRGCs)—a subpopulation of retinal
78 ganglion cells which express the photopigment melanopsin in their axons and soma (Clarke et al.,
79 2003a; Provencio et al., 2000). ipRGCs are sensitive to high intensity, short-wavelength (blue) light
80 and control non-visual functions, such as circadian photoentrainment and pupil size (Spitschan, 2019),
81 via direct projections to the suprachiasmatic nucleus of the hypothalamus and the olivary pretectal
82 nucleus (Do, 2019), respectively. The post-illumination pupil response (PIPR) describes the sustained
83 constriction of the pupil following exposure to short-wavelength light, usually relative to long-
84 wavelength light, and is assumed to be a unique non-invasive biomarker of melanopsin function in the
85 human retina (Adhikari et al., 2015; Clarke et al., 2003b; Kankipati et al., 2010). Like the flash
86 response to white light, the PIPR is researched extensively for its potential as a biomarker in various
87 ocular and neurodegenerative diseases (Chougule et al., 2019; Feigl & Zele, 2014; Kankipati et al.,
88 2011).

89 To research the PLR requires a system for illuminating the retina and measuring pupil size
90 simultaneously. For patient monitoring in critical care, hand-held pupillometers offer an attractive all-
91 in-one solution as they are portable, reliable and easy to use (Meeker et al., 2005; Taylor et al., 2003).
92 These ‘point-and-shoot’ devices are aimed at the eye to deliver a light stimulus and use infrared
93 illumination, video recording and internal algorithms to provide an instantaneous readout of PLR
94 parameters. Some limitations of automated pupillometers are that they can be expensive and
95 inflexible, offering minimal control over stimulus parameters (e.g., duration, wavelength, intensity)

SYSTEM FOR RESEARCHING THE PUPIL LIGHT REFLEX

5

96 and in some cases no access to the raw data—all of which make them less suited for scientific
97 research. Conversely, video-based eye trackers, which usually measure pupil diameter or area as part
98 of their gaze estimation pipeline, are often favoured in research for their versatility. But video-based
99 eye trackers and similar recording devices must be integrated with a system for administering light
100 stimuli. This task may not prove too challenging for basic experiments where a standard computer
101 screen will suffice, but it becomes more challenging when research calls for a bespoke setup to
102 control the spatial extent of retinal stimulation and the spectral and temporal properties of light
103 stimuli. One solution is to use a Maxwellian view pupillometry system (e.g., Adhikari et al., 2015;
104 Cao et al., 2015; Kankipati et al., 2010; Westheimer, 1966), where the light stimulus is focused onto
105 an aperture placed in front of the eye, or in the entrance plane of a pharmacologically dilated pupil,
106 and the consensual pupil response is measured from the other eye. An alternative, which does not
107 require complex optical engineering, pharmacological dilation of the pupil, or strict fixation control on
108 the part of the participant, is to use a full-field—‘Ganzfeld’—illumination system (e.g., Bonmati-
109 Carrion et al., 2018; Kardon et al., 2009); however, commercial solutions for this mode of stimulation
110 can be prohibitively expensive.

111 Here we describe *PyPlr*—a custom Python software that works with the Pupil Core (Pupil
112 Labs GmbH, Berlin, Germany) eye tracking platform to offer an affordable, versatile, extensible and
113 transparent solution for researching the PLR. Features include: 1) user-friendly and feature-rich
114 interfaces to Pupil Core, Spectra Tune Lab (STLAB: LEDMOTIVE Technologies, LLC, Barcelona,
115 Spain) light engine and Ocean Optics (Ocean Insight Inc., Oxford, UK) spectrometers, 2) flexible
116 support for alternative stimulus delivery and measurement systems, and 3) scripting tools to facilitate
117 stimulus design, optimisation and delivery, communication with respect to timing, and extraction,
118 cleaning, and analysis of pupil data. We also describe how full-field, homogenous stimulation of the
119 retina can be achieved with a low-cost integrating sphere that serves as an alternative to the more-
120 complicated Maxwellian view pupillometry setup. Following a detailed overview of the hardware and
121 the software we present two example applications as a proof of concept: 1) pupillometer-style
122 measurement and parametrisation of the PLR to a flash of white light, and 2) measuring the post-
123 illumination pupil response (PIPR) to flashes of long vs. short-wavelength light.

SYSTEM FOR RESEARCHING THE PUPIL LIGHT REFLEX

6

124

Overview

125

PyPlr is an open-source Python software for researching the PLR with the Pupil Core eye

126

tracking platform. The software, which is mapped out graphically in Figure 1, comprises a set of

127

modules for interfacing with hardware, obtaining measurements, designing and running experimental

128

protocols, and processing pupil data. The project is maintained on GitHub

129

(https://github.com/PyPlr/cvd_pupillometry) under the MIT License with extensive documentation

130

(https://pyplr.github.io/cvd_pupillometry/) and registered with the Python Package Index

131

(<https://pypi.org/project/pyplr/>) making it installable via the packaging tool *pip*.

132

A key feature of *PyPlr* is that light stimuli can be timestamped with good accuracy using the

133

Pupil Core World Camera. This feature makes it easy to integrate any light source given a suitable

134

geometry. For our own stimulation and measurement system we developed a low-cost integrating

135

sphere (see Figure 2 and description below) for use with STLAB, but *PyPlr*'s native support for

136

timestamping opens the door to many alternative solutions. In this section we present an overview of

137

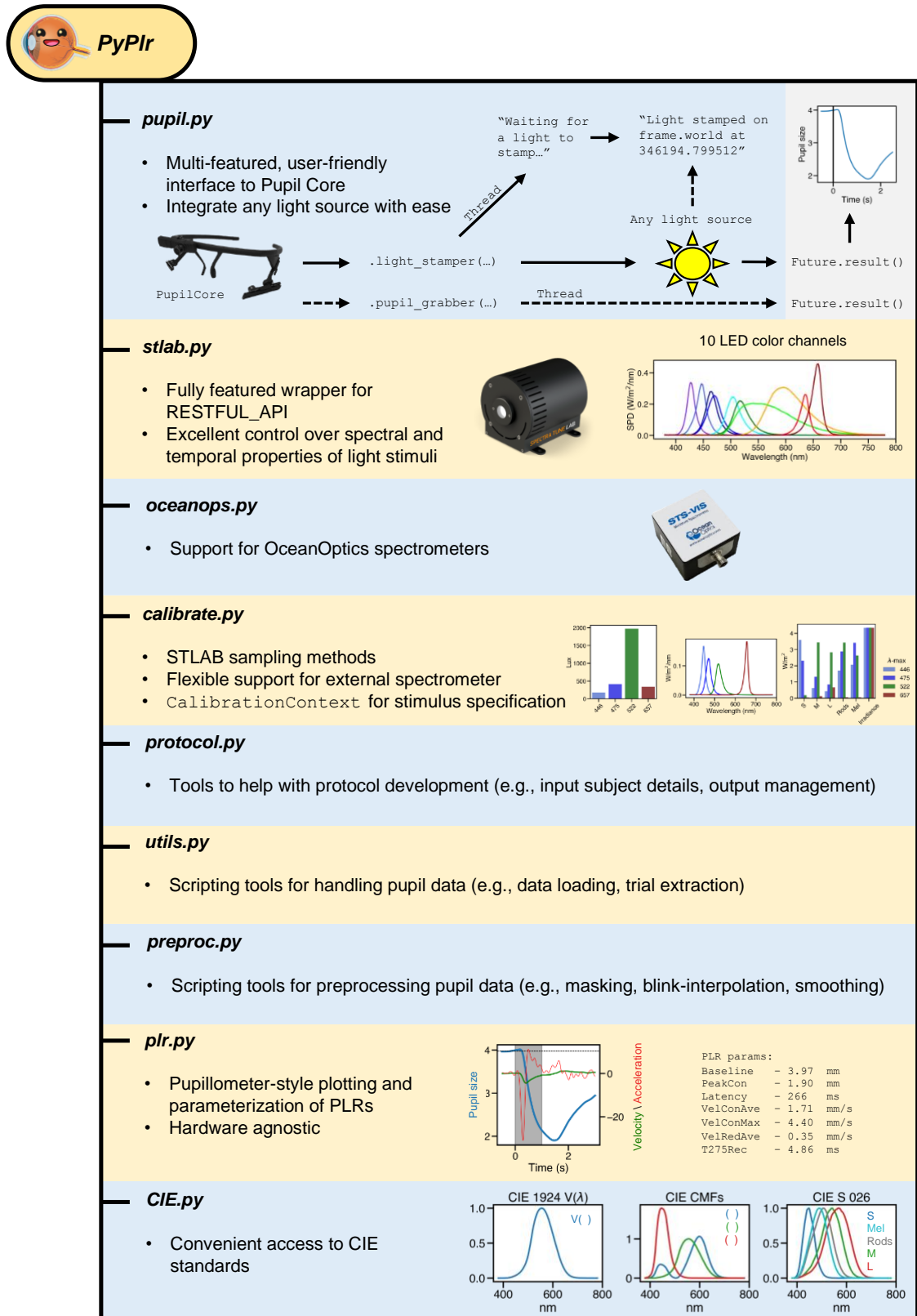
the key features of *PyPlr* and describe the low-cost integrating sphere that we built for our own

138

stimulation and measurement system.

SYSTEM FOR RESEARCHING THE PUPIL LIGHT REFLEX

7



139

140 *Figure 1. PyPIr software overview.*

SYSTEM FOR RESEARCHING THE PUPIL LIGHT REFLEX

8

141



142

143 *Figure 2.* Stimulation and measurement system: 1) integrating sphere constructed from two acrylic
144 half-domes, housed and stabilized with a wooden fixing plate, 2) inside coating of Avian-B high
145 reflectance paint to scatter light homogenously, 3) STLAB light source mounted above entry port, 4)
146 Pupil Core eye tracking headset, and 5) laptop running Pupil Capture and custom Python software.
147 The photograph was taken with the participants permission.

148 ***PyPlr* and Pupil Core**

149 *PyPlr* works with Pupil Core—an affordable, open-source, versatile, research-grade eye
150 tracking platform with high sampling rates, precise model-based 3D estimation of pupil size, and
151 many other features which make it well-suited to our application (see Kassner et al., 2014, for a
152 detailed overview of the system). In particular, Pupil Core has a Network API which supports fast and
153 reliable communication and real-time access to data via *ZeroMQ*, a universal messaging library, and
154 *MessagePack*, a binary format for information interchange. As noted above, *PyPlr* leverages the real-
155 time data streaming capabilities of Pupil Core’s forward-facing World Camera to timestamp the onset
156 of light stimuli with good temporal accuracy, opening the door to integration with virtually any light
157 source given a suitable geometry. A Pupil Core headset and its accompanying software (i.e., *Pupil*
158 *Capture*) is therefore a basic dependency of a functioning *PyPlr* setup.

159 ***pyplr.pupil.*** *PyPlr*’s *pupil.py* module greatly simplifies working with Pupil Core and its
160 Network API by wrapping all of the tricky *ZeroMQ* and *MessagePack* code into a single device class.
161 The *PupilCore* device class has a *.command(...)* method giving convenient access to all of the
162 commands available via *pupil remote*, which makes it trivially easy to connect to the eye tracker and
163 perform basic operations, such as starting and stopping a recording, calibrating, getting the current
164 pupil time, and so forth. *PupilCore* also has a rich set of class methods to facilitate the design and

SYSTEM FOR RESEARCHING THE PUPIL LIGHT REFLEX

9

165 implementation of effective pupillometry protocols. Readers are encouraged to refer to the code and
166 online documentation for detailed information on the full range of functionality. Here we describe two
167 key methods—*.light_stamper(...)* and *.pupil_grabber(...)*—and the problems they were designed to
168 solve. A minimal example of how to use *PupilCore* and its class methods to measure and plot a PLR
169 to any light stimulus is provided in Figure 3.

```
1 from time import sleep
2
3 from pyplr.pupil import PupilCore
4 from pyplr.utils import unpack_data_pandas
5
6 # Connect to Pupil Core
7 p = PupilCore()
8
9 # Start a new recording called "my_recording"
10 p.command('R my_recording')
11
12 # Wait a few seconds
13 sleep(2)
14
15 # Make an annotation for when the light comes on
16 annotation = p.new_annotation('LIGHT_ON')
17
18 # Start the .light_stamper(...) and .pupil_grabber(...)
19 lst_future = p.light_stamper(annotation=annotation, timeout=10)
20 pgr_future = p.pupil_grabber(topic='pupil.1.3d', seconds=10)
21
22 #####
23 # Administer light stimulus here #
24 #####
25
26 # Wait for the futures
27 while lst_future.running() or pgr_future.running():
28     print('Waiting for futures...')
29     sleep(1)
30
31 # End recording
32 p.command('r')
33
34 # Get the timestamp and pupil data
35 timestamp = lst_future.result()[1]
36 data = unpack_data_pandas(pgr_future.result())
37
38 # Plot the PLR
39 ax = data['diameter_3d'].plot()
40 ax.axvline(x=timestamp, color='k')
```

170

171 *Figure 3.* Minimal example demonstrating the use of the *PupilCore* device class and
172 its *.light_stamper(...)* and *.pupil_grabber(...)* methods for real-time PLR measurement. Note that it is
173 not necessary to make a recording for these methods to work, and that the script will work for any
174 light stimulus that can be detected by the World Camera (e.g., a computer screen, a light switch in a
175 dark room, an integrating sphere).

176 *.light_stamper(...)*. To extract experimental events and calculate time-critical PLR parameters
177 (e.g., constriction latency, time-to-peak constriction) requires a reliable indication in the pupil data of
178 the time at which a light stimulus was administered. The Pupil Capture software has an *Annotation*
179 *Capture* plugin which allows for samples to be labelled with an annotation manually via keypress or
180 programmatically via the Network API in a process that is analogous to sending a ‘trigger’ or ‘event
181 marker’. The obvious way to timestamp a light stimulus therefore would be to control the light source
182 programmatically from a Python script and send an annotation immediately before or after issuing a

SYSTEM FOR RESEARCHING THE PUPIL LIGHT REFLEX

10

183 command to the light; but, as a universal approach, this will likely prove far from ideal, because
184 different light sources have their own latencies which are often variable and difficult to reference. In
185 fact, our own light source (described below) takes commands via generic HTTP requests and has a
186 variable response time on the order of a few hundred milliseconds. Given that we may want to
187 calculate latency to the onset of pupil constriction after a temporally precise light stimulus, such
188 variability is unacceptable.

189 To solve the timestamping issue in a way that makes it easy to integrate *PyPlr* and Pupil Core
190 with any light source, we developed *.light_stamper(...)*—a *PupilCore* class method that uses real-time
191 data from the forward facing World Camera to timestamp the onset of a light stimulus based on a
192 sudden change in the average RGB value. The underlying algorithm simply keeps track of the two
193 most recent frames from the World Camera and sends an annotation with the timestamp of the first
194 frame where the average RGB difference exceeds a given threshold. Crucially, a *.light_stamper(...)*
195 runs in its own thread with Python's *concurrent.futures*, so the flow of execution is not blocked and
196 the result—i.e., the timestamp—is available via a call to the *.result()* method of a returned *Future*
197 object once the light has been stamped. To work properly, the *.light_stamper(...)* requires a suitable
198 stimulus geometry (the camera must be able to see the light source), an appropriately tuned threshold
199 value, and the following settings in Pupil Capture:

- 200 1) *Auto Exposure Mode* of the camera must be set to *Manual*
- 201 2) *Frame Publisher Format* must be set to *BGR*
- 202 3) *Annotation Capture* plugin must be enabled

SYSTEM FOR RESEARCHING THE PUPIL LIGHT REFLEX

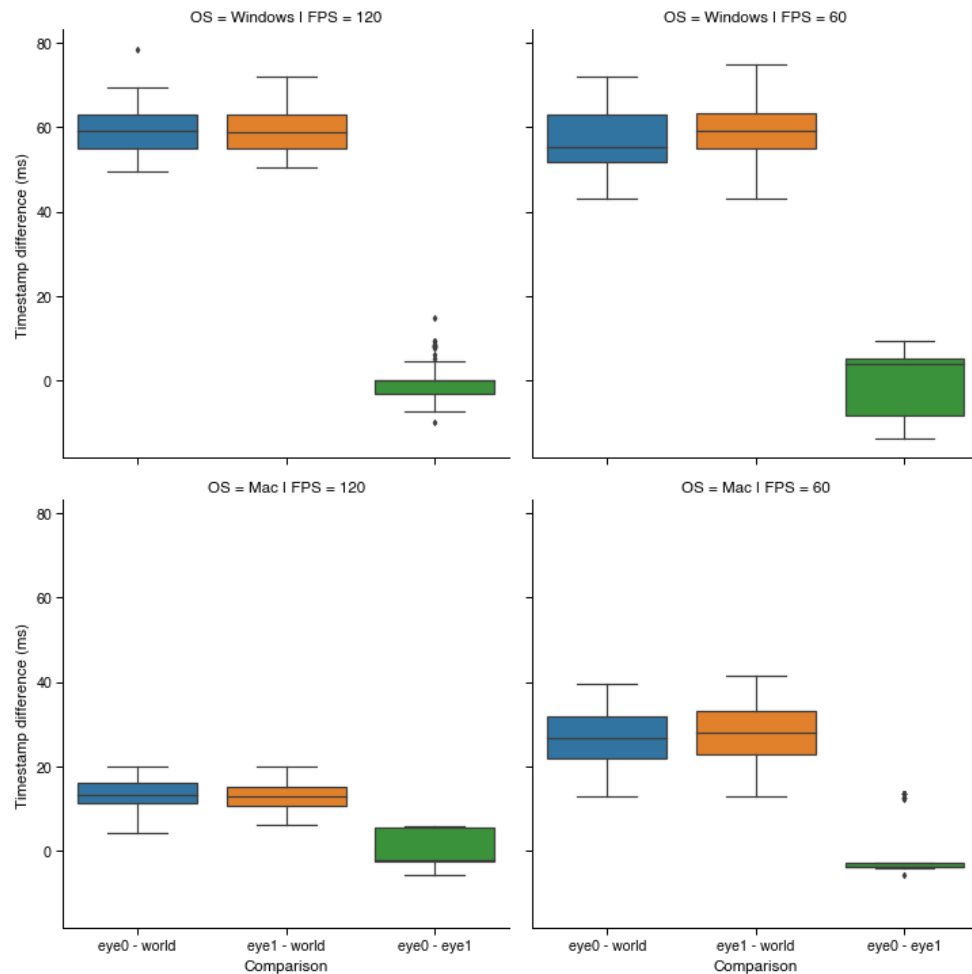
11

203 With our integrating sphere setup, we find that the *.light_stamper(...)* flawlessly captures the
204 first frame where a light becomes visible, as verified using Pupil Player and the Annotation Player
205 plugin. Timestamping accuracy therefore is limited only by camera settings (e.g., frame rate) and how
206 well the Pupil software is able to synchronise the clocks of the eye and world cameras. We were able
207 to test camera clock synchronisation by putting the Pupil Core headset inside our integrating sphere
208 (described below) and repeatedly flashing a bright orange light containing enough near infrared to
209 afford detection by the Eye cameras as well as the World camera. Prior to each flash,
210 concurrent *.light_stamper(...)*'s were instantiated, giving us the timestamp of the frame where the
211 luminance change was detected independently for each camera. Knowing from community
212 discussions that the Pupil software handles timestamps differently on Windows and Unix operating
213 systems, and more generally that frame rate will play an important role in determining the accuracy of
214 the *.light_stamper(...)*, we performed the test ($n = 100$ light flashes) on both macOS (Big Sur, 11.3.1)
215 and Windows (Windows 10) with frame rates of 60 and 120 for all cameras (Pupil Capture v3.2-20).
216 For each run of the protocol, Eye camera resolution was kept at (192, 192) with Absolute Exposure
217 Time of 25, and for the World camera, (640, 480) and 60. Auto Exposure Mode was set to 'manual
218 mode' for all cameras, and Auto Exposure Priority was disabled for the World camera.

219 The effect of frame rate and operating system on timestamping is shown in Figure 4. For both
220 macOS and Windows, the Eye camera timestamps appear well-synchronised with a margin of error
221 that is to be expected given the frame rate. On Windows, the World camera timestamps fell
222 consistently around 60 ms before the Eye camera timestamps at both 60 and 120 FPS. The same
223 pattern of a leading World timestamp was observed, though to a lesser degree, with macOS. The
224 timestamps appeared best synchronised overall on macOS with cameras running at 120 FPS, where
225 the World camera led by 15 ms on average.

SYSTEM FOR RESEARCHING THE PUPIL LIGHT REFLEX

12



226

227 *Figure 4.* Effect of operating system (OS: macOS vs. Windows) and frame rate (FPS: 60 vs. 120) on
228 timestamp differences for light flashes ($n = 100$) detected independently for each Pupil Core camera
229 with concurrent `.light_stamper(...)`'s.

230 To understand what underlies these discrepancies requires a developer's knowledge of the
231 Pupil software and its treatment of timestamps on different operating systems. At the time of writing,
232 we understand from community discussions that macOS and Linux use the hardware timestamps
233 generated by the cameras at the start of frame exposure, whereas Windows uses software timestamps
234 generated by `pyuvc` using the system's monotonic clock at the time when the frame is done
235 transferring from camera to computer. Unlike hardware timestamps, the Windows software
236 timestamps are subsequently corrected by subtracting a fixed amount of time corresponding to the
237 approximate camera latency (i.e., the difference between software and hardware timestamps), but at
238 present this procedure assumes the default resolution of the camera in question and is not optimised to
239 account for the different camera latencies associated with different resolutions (N.B., larger frames
240 take longer to transfer). This may be optimised in a future update to the Pupil software. At present, the

SYSTEM FOR RESEARCHING THE PUPIL LIGHT REFLEX

13

241 implication for our application is as follows: time-critical measures of a PLR referenced to a World
242 Camera *.light_stamper(...)* timestamp will be consistently overestimated by 15 to 60 ms, depending on
243 the operating system and camera settings being used. Though not ideal, the timestamp discrepancy is
244 at least repeatable and potentially correctable, meaning researchers are free to obtain time-critical
245 measurements of the PLR. For applications that require precise timing, researchers should perform
246 their own due diligence and engage in discussions with the Pupil Labs community to better
247 understand the timestamping implementation of the Pupil software.

248 *.pupil_grabber(...)*. The *.pupil_grabber(...)* is a *PupilCore* class method which simplifies
249 real-time access to data and empowers users to design lean applications that bypass the sometimes-
250 cumbersome record-load-export routine of the Pupil Player software. As arguments,
251 the *.pupil_grabber(...)* takes a topic string specifying the data to be grabbed (e.g., *pupil.1.3d* to grab
252 3d model data for the left eye, *pupil.* to grab all pupil data, etc.) and a numerical value specifying the
253 number of seconds to spend grabbing data. Like the *.light_stamper(...)*, the *.pupil_grabber(...)* runs in
254 its own thread with *concurrent.futures* and gives access to data via a call to the *.result()* method of a
255 returned *Future* object after the work is done. Grabbed data are stored as a list of dictionaries, which
256 can subsequently be organised into a more manageable format with the *unpack_data_pandas(...)*
257 helper function from *pyplr.utils*.

258 **Spectra Tune Lab light source**

259 As a light source for our stimulation system we chose Spectra Tune Lab (STLAB:
260 LEDMOTIVE technologies LLC, Barcelona, Spain)—a high-end, spectrally tuneable light engine
261 with ten LED colour channels, capable of generating a broad range of spectral compositions. The
262 gamut of the device and the spectral power distributions for each LED channel at maximum are
263 displayed in Figure 5 and Figure 6, respectively. STLAB connects via network cable to a small
264 computer called the Light Hub (a Beaglebone board running Linux), which in turn connects to a
265 controlling computer via USB or some network protocol (e.g., LAN, WAN, internet, etc.). STLAB
266 can be controlled programmatically with most languages via its REST API, which works with generic
267 GET and SET operations. Spectra are most easily defined by passing an array of ten 12-bit integers to

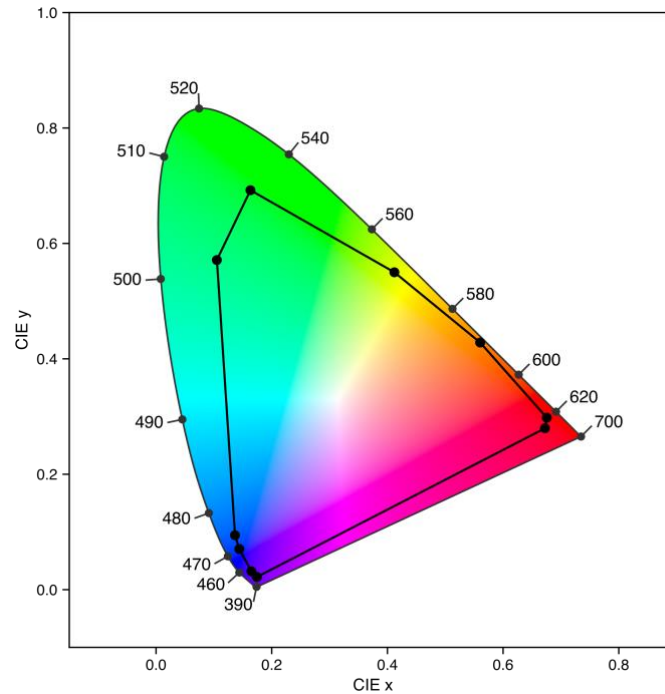
SYSTEM FOR RESEARCHING THE PUPIL LIGHT REFLEX

14

268 set the intensity of each individual LED channel. Here we describe *pyplr.stlab*, *PyPlr*'s module for

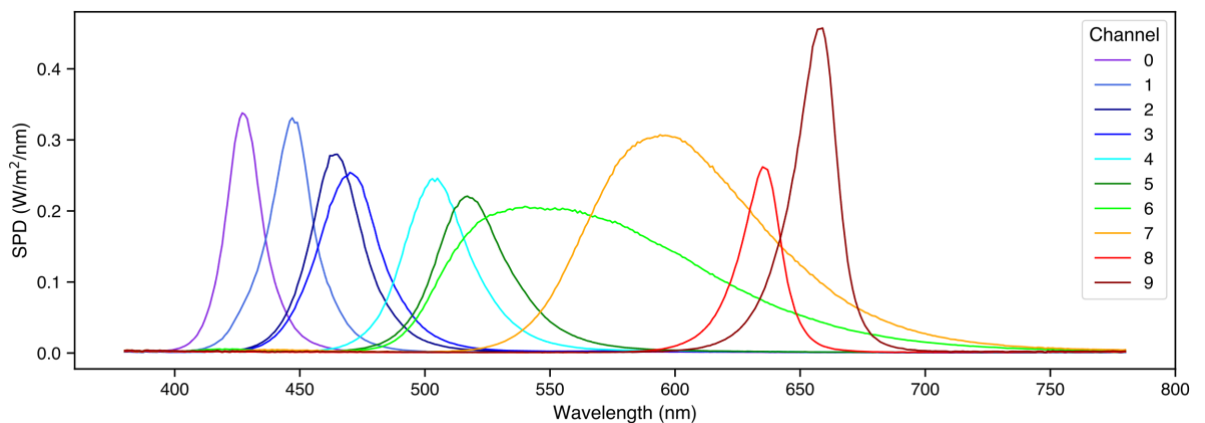
269 interfacing with STLAB, and review key aspects of performance and functionality.

270



271

272 *Figure 5.* CIE 1931 'horseshoe' chromaticity diagram (2° standard observer) for STLAB's ten LED
273 channels at maximum, defining the gamut of the stimulation system. Spectral data were obtained in a
274 darkened room with an OceanOptics STS-VIS (Ocean Insight Inc., Oxford, UK) spectrometer at the
275 plane of the integrating sphere viewing port.



276

277 *Figure 6.* Spectral power distributions for STLAB's ten LED channels at maximum. Spectral data
278 were obtained in a darkened room with an OceanOptics STS-VIS (Ocean Insight Inc., Oxford, UK)
279 spectrometer at the plane of the integrating sphere viewing port.

280 *pyplr.stlab.* This module contains *SpectraTuneLab*, a device class which uses the Python

281 *requests* library to wrap all of the functions from STLAB's REST API. Readers are encouraged to

SYSTEM FOR RESEARCHING THE PUPIL LIGHT REFLEX

15

282 check the code and documentation for further information. Additional helper functions are included to
283 assist with developing stimuli. Note that a license is required to develop against the REST API.

284 ***Device timing and video files.*** STLAB operates synchronously by default, meaning that all
285 commands sent by the Light Hub must be acknowledged before a new instruction can be processed.
286 According to the device manual, response times in this mode of operation are on the order of around
287 250 milliseconds. We verify this with our own testing, but also note that on rare occasions, perhaps
288 when the Light Hub is busy processing other tasks, the response time can be up to five s. Clearly this
289 is not suitable for administering light stimuli with exact timing. To do this, we leverage STLABs
290 asynchronous mode of operation, which allows for real-time spectral streaming with a spectral
291 switching time of less than ten milliseconds (i.e., one spectrum every ten milliseconds). This mode of
292 operation requires the advanced preparation of *video files*, which are JSON files with a particular
293 structure and the idiosyncratic DSF—*dynamic sequence file*—extension. The core inputs for making a
294 video file are a time vector to specify the spectral switching times and a separate list of spectra
295 (specified as an array of ten 12-bit integers). *pyplr.stlab* has a *make_video_file(...)* function which will
296 convert an appropriately structured *pandas* (McKinney, 2010) *DataFrame* into the required JSON
297 format and save it with a DSF extension. Also included are some higher level convenience functions
298 for quick and easy specification of timed pulse stimuli. To use video files in an experimental protocol,
299 one must simply use the *.load_video_file(...)* and *.play_video_file(...)* methods of the *SpectraTuneLab*
300 device class.

301 **Integrating sphere**

302 For some experiments it may be sufficient to perform light stimulation with a standard
303 computer monitor, but where research calls for advanced control over the geometry of retinal
304 stimulation, a bespoke setup is needed. One solution is to use a Maxwellian view pupillometry
305 system, where the light stimulus is focused onto an aperture positioned in front of the eye, or in the
306 entrance plane of a pharmacologically dilated pupil, and the consensual pupil response is measured
307 from the other eye (e.g., Cao et al., 2015). But this approach requires optical engineering and
308 resources that may not be available in the average research setting. As an alternative, we developed a
309 low-cost integrating sphere (Figure 2) that delivers a full-field—‘Ganzfeld’—stimulus and precludes

SYSTEM FOR RESEARCHING THE PUPIL LIGHT REFLEX

16

310 the need for optical engineering, pharmacological dilation of the pupil, and strict fixation control on
311 behalf of the participant.

312 **Construction.** We built the sphere from two 45-cm diameter flanged acrylic half-domes
313 (Project Plastics Ltd., Colchester, UK). The inside surfaces of the domes were cleaned, keyed with a
314 scotch pad and primed with Zinsser B-I-N Off white Matt Primer & undercoat Spray paint (William
315 Zinsser & Co. Inc., Birtley, UK) before they were sprayed with multiple coats of Avian-B high
316 reflectance paint (Avian Technologies LLC, New London, NH). The Avian-B premix was mixed on a
317 magnetic mixing plate with the correct quantities of denatured alcohol and distilled water and tested
318 for viscosity and pH in accordance with the application notes. A 28 cm opening in one of the domes
319 serves as a viewing port, and an additional 7 cm (subtending $\sim 9^\circ$ from the plane of the viewing port)
320 opening opposite the viewing port was included to allow for secondary stimuli (e.g., a fixation target)
321 or to afford exclusion of the foveal macular pigment from stimulation. On the same half of the sphere
322 as the viewing port, a 30 mm entry port for the STLAB light source was cut at an angle of 22.5-deg
323 from the top such that the diffuser of the light source could not be seen directly when looking straight
324 ahead. The sphere was stabilized on a wooden fixing plate making it suitable for placement on a desk
325 and for use with a chinrest. The raw materials for the integrating sphere cost us less than £1500.

326 **Calibration.** To create a calibrated forward model of the STLAB-sphere rig that represents
327 what an observer actually sees when looking into it, we obtained measurements with an external
328 spectrometer positioned at the plane of the viewing port. The *pyplr.calibrate* module was designed to
329 streamline this process with a *SpectraTuneLabSampler(...)* class—a sub-class of
330 *pyplr.stlab.SpectraTuneLab* with added sampling methods and support for an external spectrometer.
331 Any spectrometer with a python interface can be integrated here with minimal effort, but we used an
332 Ocean Optics STS-VIS (Ocean Insight Inc., Oxford, UK), which has native support from
333 *pyplr.oceanops* via the *Seabreeze* (v1.3.0; Poehlmann, 2019) Python library. It would take a long time
334 to sample every possible device setting, so we opted to sample the 12-bit intensity range in a dark
335 room, independently for each LED channel in steps of 65, which amounts to 63 evenly spaced
336 measurements per LED. Figure 7 shows how easy it was to obtain these spectral data.

SYSTEM FOR RESEARCHING THE PUPIL LIGHT REFLEX

17

```
1 from pyplr.calibrate import SpectraTuneLabSampler
2 from pyplr.oceanops import OceanOptics
3
4 # Connect to devices
5 oo = OceanOptics.from_first_available()
6 d = SpectraTuneLabSampler(password='*****', external=oo)
7
8 # Specify LEDs and intensities to be sampled
9 leds = [0, 1, 2, 3, 4, 5, 6, 7, 8, 9]
10 intensities = [i for i in range(0, 4096, 65)]
11
12 # Sample
13 d.sample(leds=leds,
14          intensities=intensities,
15          external=oo,
16          randomise=True)
17 d.make_dfs(save_csv=True)
```

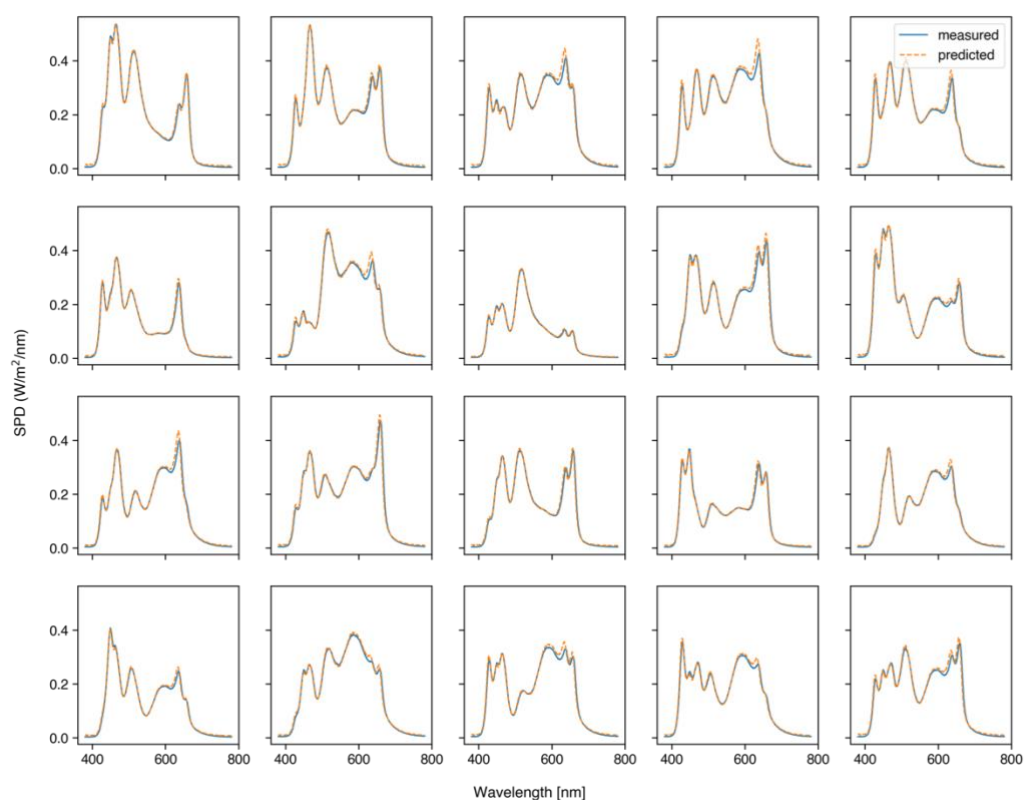
337

338 *Figure 7. Profiling the integrating sphere with `pyplr.calibrate` and `pyplr.oceanops`. Measurements*
339 *were obtained in a dark room with an OceanOptics STS-VIS (Ocean Insight Inc., Oxford, UK)*
340 *spectrometer fitted with a cosine corrector and positioned at typical eye position.*

341 Having obtained the raw spectral measurements with our OceanOptics spectrometer, a
342 device-specific calibration pipeline was implemented to account for the effect of PCB temperature
343 and integration time on raw sensor readings. The calibrated spectral data were then passed to
344 `pyplr.calibrate.CalibrationContext`, a data-handling class which uses reindexing and linear
345 interpolation to fill in the gaps and automatically generate lookup tables giving easy access to the
346 predicted spectral power distribution, *a*-opic irradiances, lux, and unweighted irradiance for all
347 possible combinations of LED-intensity settings. Crucially, the `CalibrationContext` also has
348 a `.predict_spd(...)` method which will predict the spectral output from a list of ten 12-bit values, as
349 taken by STLAB. There is also a `.fit_curves(...)` method that fits beta cumulative distribution
350 functions to the LED-intensity data, and an `.optimise(...)` method that applies the resulting parameters
351 to correct a stimulus profile for any departures from linearity. Figure 8 shows how spectra can be
352 accurately predicted from the `CalibrationContext` and Figure 9 demonstrates the linearity of the
353 relationship between STLAB's input and output.

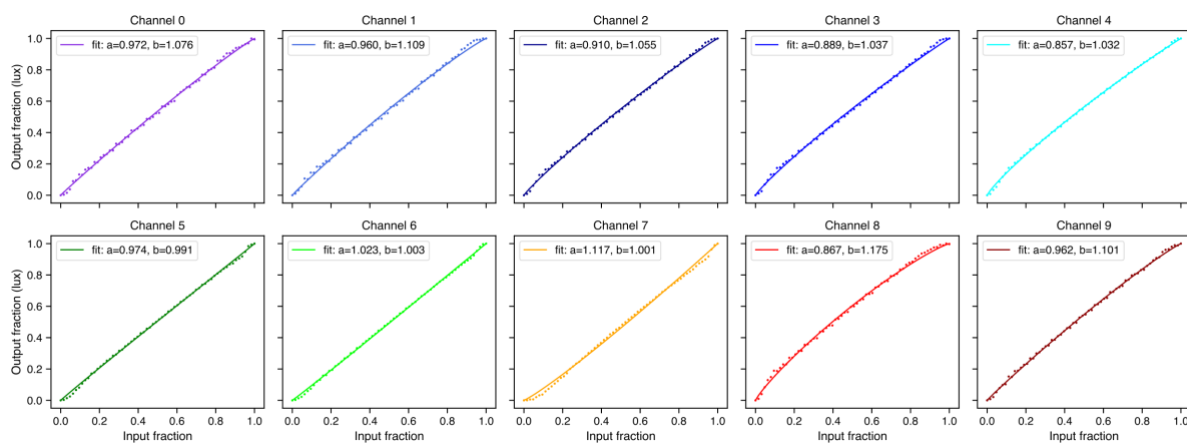
SYSTEM FOR RESEARCHING THE PUPIL LIGHT REFLEX

18



354

355 *Figure 8.* Measured spectral power distributions for 20 random device settings compared with the
356 spectral power distributions as predicted by the *CalibrationContext.predict_spd(...)* method using the
357 same settings. The 20 random spectra were measured with the same spectrometer and under the same
358 conditions as the calibration spectra.



359

360 *Figure 9.* Output of the *CalibrationContext.fit_curves(...)* method, showing the relationship between
361 input (12-bit) and output (photopic illuminance in lx) for all of STLAB's LED channels as measured
362 by our OceanOptics STS-VIS (Ocean Insight Inc., Oxford, UK).

SYSTEM FOR RESEARCHING THE PUPIL LIGHT REFLEX

19

363 **Safety.** We evaluated the safety of the stimulation system in accordance with the British
364 Standards Document on the Photobiological Safety of Lamps and Lamp Systems (BS EN 62471:
365 British Standards Institute, 2008). Section 4.1 (Annex ZB, page 40) of the BS EN 62471 states that
366 ‘Detailed spectral data is required if the luminance of the source exceeds 10^4 cd/m^2 ’. Initial scoping
367 measurements collected with a Photo Research SpectraScan PR-670 for all LEDs at 100% gave a
368 luminance reading of 18000 cd/m^2 at the plane of the viewing port. The maximum output of our
369 stimulation system therefore exceeded this specification, so we obtained detailed spectral
370 measurements. Section 4.3.3 of the BS EN 62471 states:

371 To protect against retinal photochemical injury from chronic blue-light exposure, the
372 integrated spectral radiance of the light source weighted against the blue-light hazard
373 function, $B(\lambda)$, i.e., the blue light weighted radiance, L_B , shall not exceed the levels defined
374 by:

$$375 \quad L_B \cdot t = \sum_{300}^{700} \sum_t L_\lambda(\lambda, t) \cdot B(\lambda) \cdot \Delta t \cdot \Delta \lambda \leq 106 \text{ J} \cdot \text{m}^{-2} \cdot \text{sr}^{-1} \text{ (for } t \leq 10^4 \text{ s)}$$

$$376 \quad L_B = \sum_{300}^{700} \sum_t L_\lambda \cdot B(\lambda) \cdot \Delta \lambda \leq 100 \text{ W} \cdot \text{m}^{-2} \cdot \text{sr}^{-1} \text{ (for } t > 10^4 \text{ s)}$$

377 Where:

378 $L_\lambda(\lambda, t)$ is the spectral radiance in $\text{W} \cdot \text{m}^{-2} \cdot \text{sr}^{-1} \cdot \text{nm}^{-1}$

379 $B(\lambda)$ is the blue-light hazard weighting function

380 $\Delta \lambda$ is the bandwidth in nm

381 t is the exposure duration in seconds. (p. 44)

382 Using the minimum radiance limit for the retinal blue light hazard exposure limit, given as $100 \text{ W} \cdot$
383 $\text{m}^{-2} \cdot \text{sr}^{-1}$ for exposures of greater than 10000 s, we note that our source is below the retinal blue light
384 hazard exposure limit. These findings were confirmed by processing the data with “EyeLight”, an
385 Optical Safety Software Platform supplied by Blueside Photonics Ltd. (Preston, UK) and the National
386 Physical Laboratory (Teddington, UK). However, given that our stimulation system may be used in a
387 dark room following a period of dark adaptation, pupil diameter will be greater than 3 mm at the start
388 of exposure. Section 4.2.1 of the BS EN 62471 states:

SYSTEM FOR RESEARCHING THE PUPIL LIGHT REFLEX

20

389 When the luminance of the source is adequately high ($>10 \text{ cd}\cdot\text{m}^{-2}$), and the exposure duration
390 is greater the 0.25s, a 3mm pupil diameter (7mm^2 area) was used to derive the exposure limit.

391 (Annex ZB, p. 40)

392 To take this into account we applied a pupil correction factor of 6 (pupil ratio: $\left(\frac{7}{3}\right)^2 = 5.4$), which
393 reduces the retinal blue light hazard exposure limit to $16.6 \text{ W}\cdot\text{m}^{-2}\cdot\text{sr}^{-1}$. Therefore, when running the
394 source at 100% and applying a safety factor to correct for the pupil size, our stimulation system is
395 above the radiance retinal blue light hazard exposure limit value of $100 \text{ W}\cdot\text{m}^{-2}\cdot\text{sr}^{-1}$ for an exposure of
396 10000 s. From this analysis we conclude that our system is safe for all our intents and purposes.

397 Researchers considering prolonged exposure to short wavelengths should consult the relevant
398 standards and ensure that their stimuli do not exceed the retinal blue light hazard exposure limit.

399 **Data analysis**

400 There is more than one valid approach to the analysis of pupillometry data, but the optimal
401 approach will depend on the type of experiment being run, the quality of the data, and the research
402 question in mind. Kelbsch et al. (2019) give an informative view on standards in pupillometry of the
403 light reflex and many papers offer advice on best practices and specific issues to do with data analysis
404 (e.g., Hayes & Petrov, 2015; Kret & Sjak-Shie, 2019; Mathôt, 2017; Sirois & Brisson, 2014; Winn et
405 al., 2018), much of which is embodied in community-developed packages that aim to streamline the
406 processing and analysis of pupillometry data (e.g., Acland & Braver, 2014; Mittner, 2020).

407 Ultimately, data analysis is a personal choice, and researchers would do well to explore the options
408 that are available. That said, *PyPlr* includes a set of pandas-reliant scripting tools for implementing a
409 standard data processing pipeline that is optimised to study the PLR and to account for some of the
410 idiosyncrasies of Pupil Labs data. These tools are organised into three separate modules: *pyplr.utils*
411 has tools for loading data and extracting trials; *pyplr.preproc* has tools for masking, interpolating and
412 filtering pupil data; and *pyplr.plr* supports pupillometer-style plotting and parametrisation of PLR
413 data. These tools are in continuous development and will evolve over time, hopefully with
414 contributions from other active researchers.

SYSTEM FOR RESEARCHING THE PUPIL LIGHT REFLEX

21

415

Examples

416 We now offer two example applications of *PyPlr* and our own custom-built stimulation and
417 measurement system. In the first example, we obtain repeated measurements of the PLR to a white
418 light stimulus and compare the results with those from an industry-leading automated pupillometer. In
419 the second, we measure the PIPR to long and short wavelength light.

420 Simple PLR

421 Automated pupillometers are the standard instruments for measuring the PLR. These
422 handheld devices are aimed at the eye to deliver a light stimulus and use infrared video recording and
423 internal algorithms to provide an instant readout of the PLR and its associated parameters. The PLR-
424 3000 (NeurOptics, Laguna Hills, CA, USA) is a leading example with established intraoperator
425 reproducibility and normative benchmarks (Asakawa & Ishikawa, 2017; Winston et al., 2019), access
426 to raw data, and the flexibility to define stimulation protocols by adjusting the pulse intensity,
427 background intensity, measurement duration, pulse duration and pulse onset time. Our system is no
428 competition for the compactness, portability and ease of use of an automated pupillometer like the
429 PLR-3000, but here we demonstrate how it can be made to function in a similar way and to yield
430 comparable results.

431 Method.

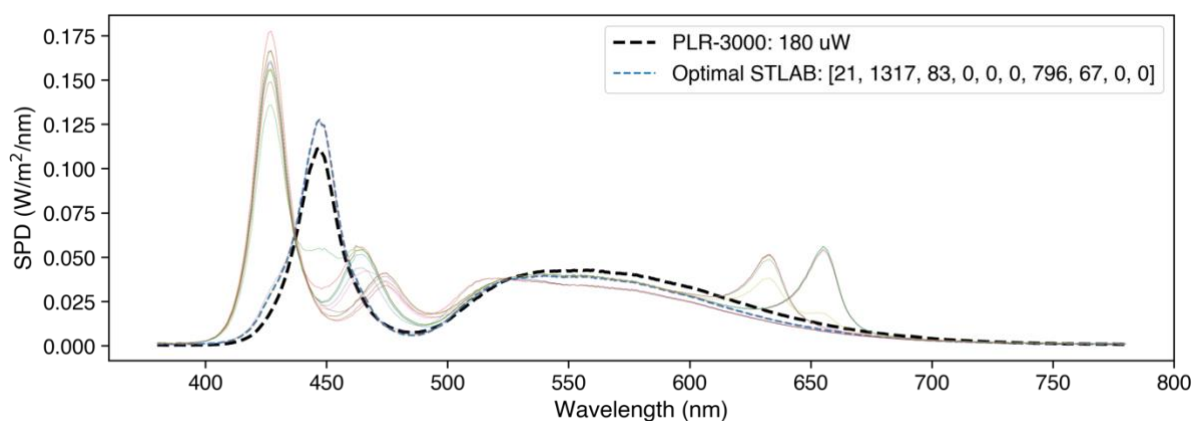
432 **Participants.** Two non-naive subjects took part in this study, which was approved by The
433 University of Oxford's central research ethics committee (R54409/RE005). Both participants had
434 normal colour vision, as assessed by The New Richmond HRR Pseudoisochromatic Test for Colour
435 Vision (Cole et al., 2006).

436 **Stimulation protocols.** A PLR-3000 (NeurOptics, Laguna Hills, CA, USA) automated
437 pupillometer was configured to record nine seconds of data and to deliver a one second pulse (180
438 uW) against a dark background after one second of recording. A comparable stimulus for STLAB was
439 generated by obtaining spectral measurements of the PLR-3000 stimulus—produced by four white
440 LEDs—with an OceanOptics STS-VIS (Ocean Insight Inc., Oxford, UK) spectrometer at the usual
441 eye position and then using linear algebra to find the STLAB settings required to produce a spectrum
442 matched for *a*-opic (S-cone-opic, M-cone-opic, L-cone-opic, rhodopic and melanopic) irradiance

SYSTEM FOR RESEARCHING THE PUPIL LIGHT REFLEX

22

443 (CIE, 2018: see Figure 10). The optimal settings were then used to make a one second pulse stimulus
444 for STLAB, which was administered from a Windows laptop running Pupil Capture (v3.2-20) and a
445 custom Python script designed to mimic the functionality of the PLR-3000. Pupil Core Eye camera
446 resolution was kept at (192, 192) with Absolute Exposure Time of 25, and the corresponding settings
447 for the World camera were (640, 480) and 60. Auto Exposure Mode was set to ‘manual mode’ for all
448 cameras, and Auto Exposure Priority was disabled for the World camera.



449

450 *Figure 10.* Spectral power distributions of the PLR-3000 white light stimulus and *a*-opic irradiance-
451 matched STLAB-sphere stimulus. We defined the optimal settings as those which produce a spectrum
452 with the least squared error, although in theory it should not matter which is used. Colored lines show
453 alternative solutions to the stimulus matching problem.

454 **Testing procedure.** Testing took place in a dark room where the light from the computer
455 monitor was the only source of illumination. Twenty PLRs were measured alternately with each
456 system. PLR-3000 measurements were obtained from the right eye and following the manufacturer’s
457 standard guidelines and Pupil Core measurements were obtained from the left eye. For the STLAB-
458 sphere PLRs, eye level was maintained with a chinrest at the vertical centre of the viewing port and an
459 eye patch was worn over the right eye to ensure dose equivalence with the monocular PLR-3000
460 stimulus. Participants were asked to look straight ahead, to maintain steady fixation, and to refrain
461 from blinking during the recording. If poor results were obtained for any measurement with either
462 system, the measurement was repeated after a short break.

463 **Data analysis.** PLR-3000 data were obtained from the device via Bluetooth, converted to
464 CSV format and then processed with custom Python software. Invalid samples (marked as 0 in the
465 data file) were masked and reconstructed with linear interpolation. Our custom *PyPlr* application

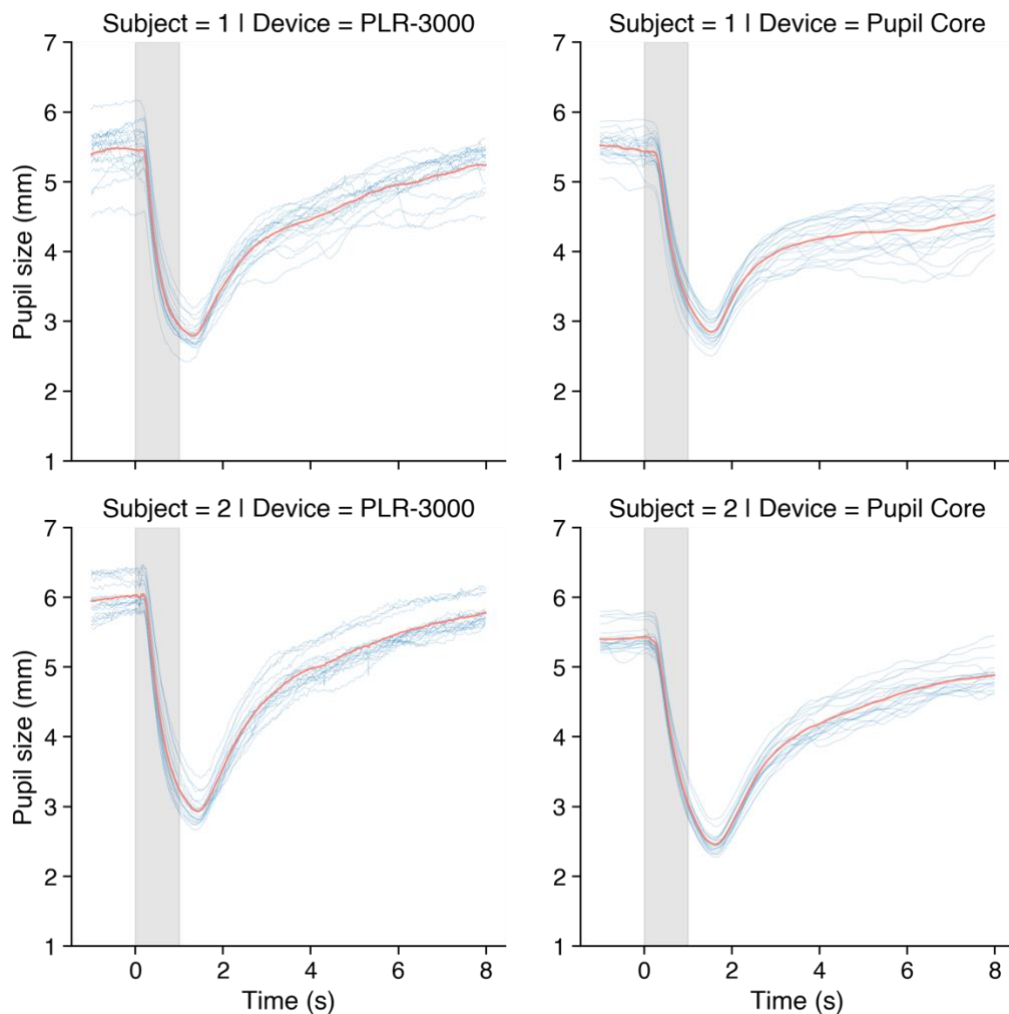
SYSTEM FOR RESEARCHING THE PUPIL LIGHT REFLEX

23

466 collected data in real-time using the *.light_stamper(...)* and *.pupil_grabber(...)* methods. High
467 frequency noise was removed with a 3rd order Butterworth filter (4 Hz cut-off) before parameters were
468 calculated with *pyplr.plr.PLR*. Raw data and parameters for each measurement were saved in CSV
469 format. Subject 1 failed to reach 75% recovery within the measurement period on two trials with the
470 PLR-3000 and on 16 trials with the integrating sphere. These trials were treated as ‘not-a-number’
471 values in the averaging procedure.

472 **Results.** The PLR measurements ($n = 20$) obtained with the PLR-3000 and with our own
473 system were comparable for both subjects (Figure 11). The PLR parameters calculated for both
474 systems, shown in

475 Table 1, were also generally comparable.



476

477 *Figure 11.* Comparison of PLR measurements ($n = 20$) obtained with a PLR-3000 and our own
478 stimulation and measurement system. Note that the Pupil Core data were filtered with a 3rd order
479 Butterworth filter (4 Hz cut-off).

SYSTEM FOR RESEARCHING THE PUPIL LIGHT REFLEX

24

480

481 *Table 1.* Mean and standard deviation of PLR ($n = 20$) parameters as calculated by a NeurOptics PLR-
 482 3000 (NeurOptics, Laguna Hills, CA, USA) and *PyPlr*. Different naming conventions are used to
 483 emphasize that our parameter calculation principles may differ to those used by the PLR-3000. Note
 484 that *pyplr.plr.PLR* calculates other parameters as well.

NeurOptics							
Subject	Init	End	LAT	ACV	MCV	ADV	T75 [†]
1	5.44 (0.35)	2.78 (0.17)	0.216 (0.02)	-3.54 (0.31)	-6.12 (0.48)	1.03 (0.20)	3.80 (1.22)
2	6.02 (0.21)	2.94 (0.18)	0.228 (0.01)	-3.46 (0.22)	-5.76 (0.40)	1.13 (0.17)	3.55 (0.55)
PyPlr							
	Baseline	PeakCon	Latency*	VConAve	VConMax	VRedAve	T75Rec [†]
1	5.51 (0.19)	2.85 (0.17)	0.301 (0.05)	-1.98 (0.15)	-4.68 (0.33)	0.35 (0.04)	5.81 (0.45)
2	5.40 (0.17)	2.45 (0.13)	0.309 (0.01)	-2.11 (0.15)	-4.55 (0.33)	0.41 (0.04)	4.17 (1.11)

485 *Note:* PLR-3000 parameter definitions: Init, maximum pupil size before constriction; End, pupil
 486 diameter at peak constriction; LAT, time of onset of constriction following initiation of the light
 487 stimulus; ACV, average velocity of how the pupil diameter is constricting measured in millimeters per
 488 second; MCV, maximum velocity of how the pupil diameter is constricting measured in millimeters
 489 per second; ADV, the average pupillary velocity when, after having reached the peak of constriction,
 490 the pupil tends to recover and to dilate back to the initial resting size, measured in millimeters per
 491 second; T75, the time taken by the pupil to recover 75% of the initial resting pupil size after it has
 492 reached the peak of constriction. * We defined latency as the time difference between
 493 the *.light_stamper(...)* timestamp and the negative acceleration peak of the initial pupil constriction
 494 (see Bergamin & Kardou, 2003). Note also that these latency values were derived from measurements
 495 taken on a Windows laptop, and therefore that they include ~59 ms of timestamping error (see Figure
 496 4). † Subject 1 failed to reach 75% recovery within the measurement period on two trials with the
 497 PLR-3000 and on 16 trials with the integrating sphere. Subject 2 failed to reach 75% recovery on one
 498 trial with the integrating sphere. These trials were treated as ‘not-a-number’ values in the averaging
 499 procedure.

500 **Discussion.** Here we show that our *PyPlr* stimulation and measurement system can function
 501 like an industry-leading automated pupillometer. Both systems were configured to record nine
 502 seconds of data and to deliver one second pulses of white light stimuli matched for *a*-opic-irradiance
 503 (Figure 10). The resulting PLR traces were highly comparable between systems in terms of absolute
 504 measurement units and variability. The PLR-3000 device yields seven parameters for every measured
 505 pupil trace, an aspect of functionality that we were able to mimic with *pyplr.plr.PLR* (see
 506 Table 1). Despite alternative approaches to calculating the parameters, the averages and
 507 standard deviations were generally similar. The most marked discrepancies were between the
 508 parameters representing constriction latency and the time taken for the pupil to recover to 75% of the

SYSTEM FOR RESEARCHING THE PUPIL LIGHT REFLEX

25

509 baseline value after reaching peak constriction. Regarding latency, we note that the *PyPlr* data were
510 collected on a Windows laptop and therefore that they include on average ~59 ms timestamping
511 error¹. Subtracting 59 ms from the averages for Subjects 1 and 2 gives values of 242 ms and 250 ms,
512 respectively, which are more plausible with respect to normative values in the literature (e.g., Shah et
513 al., 2020; Straub et al., 1992; Winston et al., 2019). For the 75% metric, the discrepancy may be
514 explained by geometrical differences in retinal stimulation: Although the stimuli were matched for α -
515 opic irradiance and delivered monocularly, the PLR-3000 light stimulus comes from 4 small LEDs,
516 whereas our integrating sphere stimulates the entire visual field. This may have altered the extent to
517 which the pupil response was driven by melanopsin excitation, which in turn could explain why
518 Subject 1 failed to reach 75% recovery on 16/20 trials with the sphere but only 2/20 trials with the
519 PLR-3000.

520 Although subtracting 59 ms from our latency measures gives plausible values, we do not
521 advocate for this as a blanket solution. Rather, we point out that the ground truth for constriction
522 latency is difficult to obtain and that measurements are constrained by hardware and calculation
523 principles. For example, with video recording at 30 and 120 frames per second, precision is limited to
524 33.333 ms and 8.333 ms, respectively, although this may be improved somewhat by up sampling the
525 data prior to calculation (e.g., see Bergamin & Kardon, 2003). Similarly, latency measures based on
526 the negative acceleration peak of pupil constriction (e.g., Bergamin & Kardon, 2003) will differ to
527 those based on the time taken to cross a threshold of change from baseline (e.g., Maynard et al.,
528 2015). Repeatability is what ultimately matters in this domain, and our data suggest that both the
529 PLR-3000 (NeuroOptics, Laguna Hills, CA, USA) and Pupil Core (Pupil Labs GmbH, Berlin,
530 Germany) systems perform well in this regard.

531 **PIPR**

532 Whereas the PLR refers to the general response of the pupil to light, the PIPR describes the
533 sustained constriction of the pupil following exposure to short wavelength (blue) light and is assumed
534 to be a unique non-invasive signature of melanopsin processing in the human retina. As an optimum

¹ This corresponds to the average difference between the World and Eye camera timestamps in Figure 4 for OS = Windows | FPS = 120.

SYSTEM FOR RESEARCHING THE PUPIL LIGHT REFLEX

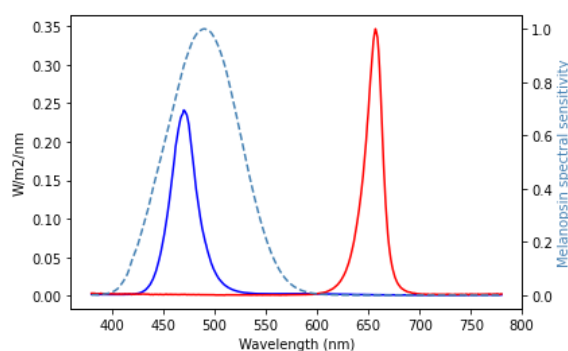
26

535 protocol for measuring the PIPR, Park et al. (2011) recommend comparing pupil responses to high
536 intensity ($2.6 \log \text{cd/m}^2$) one-second pulses of short and long wavelength light presented in darkness
537 following a period of dark adaptation. Park et al. obtained their PIPR measurements with the industry-
538 leading Espion V5 system with ColorDome LED full-field stimulator (Diagnosys LLC, Lowell, MA).
539 Here we describe a comparable protocol for measuring the PIPR with our own stimulation and
540 measurement system.

541 **Method.**

542 **Participants.** The same participants as previous took part in this study.

543 **Stimulation protocols.** Stimuli were administered via STLAB's fourth (blue, $\lambda\text{-max} = 470$)
544 and tenth (deep red, $\lambda\text{-max} = 657$) LED channels, which offer maximal and minimal melanopic
545 excitation, respectively. The blue stimulus was set at $\sim 800 \text{ lx}$ and the red stimulus was matched for
546 unweighted irradiance. The spectral power distributions of the stimuli are visualised in Figure 12
547 along with the spectral sensitivity curve for melanopsin. Both were presented for one second using
548 STLAB video files.



549

550 *Figure 12.* Spectral power distributions of PIPR stimuli shown in relation to the relative energy
551 spectral sensitivity curve for melanopsin.

552 **Testing procedure.** Participants completed the PIPR protocol in a dark room after 20 min
553 dark-adaptation. When ready to begin, they placed their chin on the chinrest and the experimenter
554 ensured that their eyes were level with the vertical centre of the viewing port. Participants were asked
555 to roll their eyes as the experimenter ensured a good fit of the 3D eye models in the Pupil Capture and
556 were then asked to look straight ahead for the duration of the recording. The recording lasted $\sim 12 \text{ min}$,
557 during which time three of each colour light stimulus were administered in a random order with ~ 2

SYSTEM FOR RESEARCHING THE PUPIL LIGHT REFLEX

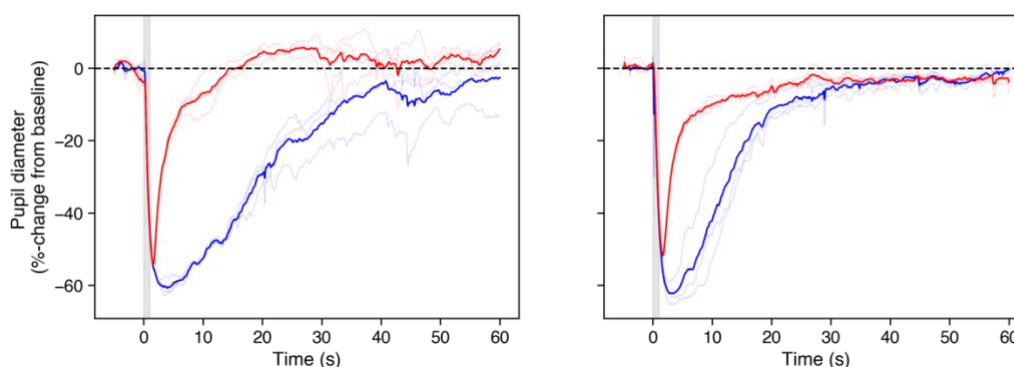
27

558 min spacing. A high-pitched beep signalled to the participant that a stimulus would be presented in the
559 next five-to-ten s, and a low-pitched beep indicated that one min had passed since the stimulus.
560 Recording was binocular at 120 Hz and light stimuli were timestamped using the *.light_stamper(...)*
561 method.

562 **Data analysis.** Data were exported to CSV format via the Pupil Player software and processed
563 with scripting tools from *pyplr.utils* and *pyplr.preproc*. For each participant, the eye with the highest
564 average confidence was chosen for analysis. To account for blinks, pupil data were masked with ‘not-
565 a-number’ values where the first derivative exceeded ± 3 SD or if the corresponding confidence value
566 was below .95. The missing data were reconstructed with linear interpolation before the time-course
567 was smoothed with a third-order Butterworth filter (4 Hz cut-off). Using the *.light_stamper(...)*
568 timestamps, 65 seconds of pupil data were then extracted for each stimulus event and converted to %-
569 change from a baseline calculated as the average pupil diameter in the five seconds prior to stimulus
570 onset.

571 **Results.** Clear PIPRs were observed for both subjects (see Figure 13).

572



573

574 *Figure 13.* Average PIPRs for Subject 1 (left) and Subject 2 (right). Desaturated lines show individual
575 trials.

576 **Discussion.** Here we show that our system of hardware and software can be used to measure
577 the PIPR in a way that compares to industry-leading commercial equipment (e.g., Lei et al., 2014;
578 Park et al., 2011; Romagnoli et al., 2020). It is worth noting that many aspects of this protocol are
579 customisable. For example, the duration, intensity and spectral composition of the stimulus can be
580 specified in accordance with the limits imposed by STLAB. Further, rather than administering simple

SYSTEM FOR RESEARCHING THE PUPIL LIGHT REFLEX

28

581 light pulses, one could generate flicker stimuli, or stimuli which modulate sinusoidally in intensity.
582 Such stimuli have been used previously to probe the temporal characteristics of melanopsin's and
583 other photoreceptor's contributions to pupil control (e.g., Joyce et al., 2015, 2018; Maynard et al.,
584 2015; Rukmini et al., 2019; Spitschan et al., 2014).

585 **General discussion**

586 In this paper we have described *PyPlr*—a *pip* installable Python software for researching the
587 PLR with the Pupil Core eye tracking platform. A key feature of *PyPlr* is its feature rich, object-
588 oriented interface to Pupil Core which includes a *.light_stamper(...)* method for accurate
589 timestamping of any light stimulus given a suitable geometry, and a *.pupil_grabber(...)* method which
590 simplifies real-time access to pupil data. The *.light_stamper(...)* works flawlessly with our own
591 integrated system and we can confirm that it also works with other light sources, such as a computer
592 monitor controlled by *PsychoPy* and a light switch in a dark room (see online documentation for
593 examples). *PyPlr* also has native support for our chosen light stimulation and measurement hardware
594 (STLAB and OceanOptics STS-VIS) as well as tools for streamlining the processing and analysis of
595 pupillometry data. As such, *PyPlr* in combination with Pupil Core is a versatile, extensible and
596 comparatively affordable solution to researching the PLR.

597 In addition to the software, we have described a low-cost integrating sphere stimulation rig
598 which delivers full field, “Ganzfeld”, light stimulation. The integrating sphere provides good control
599 over the geometry of retinal stimulation without the need for a complex Maxwellian view optical
600 setup. The raw materials for our sphere cost us less than £1500, which is a small fraction of the price
601 of an equivalent commercial solution. We use our sphere with an STLAB light engine, giving us a
602 high level of control over the temporal and spectral properties of light stimuli, and we calibrated the
603 system with an OceanOptics STS-VIS spectrometer placed at the normal eye position. Prospective
604 users may wish to develop for alternative stimulation and measurement hardware, in which case their
605 contributions to the software would be greatly appreciated.

606 We gave two examples showing how our complete integrated setup can rival industry leading
607 commercial equipment for measuring the PLR and PIPR. In the PLR example, our integrated system
608 was made to function like an automated pupillometer, administering a flash of white light and saving

SYSTEM FOR RESEARCHING THE PUPIL LIGHT REFLEX

29

609 raw data, a plot, and parameters of the PLR. In terms of absolute units and variability, the PLR
610 measurements and parameters were comparable to those obtained with an industry leading automated
611 pupillometer (PLR-3000, NeurOptics, Laguna Hills, CA, USA) under the same stimulus and testing
612 conditions. Likewise, we were able to obtain measurements of the PIPR which rival those made with
613 industry-leading commercial equipment (e.g., Lei et al., 2014; Park et al., 2011; Romagnoli et al.,
614 2020). Of note, these two examples represent only a snapshot of our systems capabilities, and the
615 scope for further stimulation and measurement protocols is limited only by the capabilities of Pupil
616 Core and the chosen light source. For example, with STLAB's 10 LED channels, one could
617 potentially design protocols which use the method of silent substitution to examine the contribution of
618 individual photoreceptor classes to pupil control (e.g., see Spitschan & Woelders, 2018).

619 In summary, *PyPlr* and Pupil Core offer an affordable, flexible, research-grade solution for
620 measuring the PLR. We hope that other researchers will find it useful and contribute to its
621 development.

622 **Acknowledgements**

623 We thank Grahame Faulkner and David Sliney for guidance on light safety, Chris Gibbs,
624 Chris Hatcher, David Ilsley and Duncan Constable for building the stimulation rig, Thibault Lestang
625 and the Oxford Research Software Engineering (OxRSE) Group for helpful advice at various stages
626 of software development, and Pablo Prietz and the Pupil Labs community for support on Discord.

627 **Open Practices Statement**

628 The data and materials for all experiments are available at <https://zenodo.org/record/4785288>.

629 None of the experiments were preregistered.

630

SYSTEM FOR RESEARCHING THE PUPIL LIGHT REFLEX

30

631

References

- 632 Acland, B. T., & Braver, T. S. (2014). *Cili (v0.5.3) [computer software]*.
- 633 Adhikari, P., Zele, A. J., & Feigl, B. (2015). The post-illumination pupil response (PIPR).
- 634 *Investigative Ophthalmology and Visual Science*, 56(6), 3838–3849.
- 635 <https://doi.org/10.1167/iovs.14-16233>
- 636 Bitsios, P., Prettyman, R., & Szabadi, E. U. (1996). Changes in autonomic function with age: A study
- 637 of pupillary kinetics in healthy young and old people. *Age and Ageing*, 25(6), 432–438.
- 638 <https://doi.org/10.1093/ageing/25.6.432>
- 639 Bonmati-Carrion, M. A., Hild, K., Isherwood, C. M., Sweeney, S. J., Revell, V. L., Madrid, J. A., Rol,
- 640 M. A., & Skene, D. J. (2018). Effect of single and combined monochromatic light on the human
- 641 pupillary light response. *Frontiers in Neurology*, 9(NOV), 1–15.
- 642 <https://doi.org/10.3389/fneur.2018.01019>
- 643 British Standards Institute. (2008). *Photobiological safety of lamps and lamp systems (BS EN 62471)*.
- 644 Cao, D., Nicandro, N., & Barrionuevo, P. A. (2015). A five-primary photostimulator suitable for
- 645 studying intrinsically photosensitive retinal ganglion cell functions in humans. *Journal of Vision*,
- 646 15(1), 1–13. <https://doi.org/10.1167/15.1.27>
- 647 Chen, J., Gombart, Z., Rogers, S., Gardiner, S., Cecil, S., & Bullock, R. (2011). Pupillary reactivity as
- 648 an early indicator of increased intracranial pressure: The introduction of the neurological pupil
- 649 index. *Surgical Neurology International*, 2(1), 82. <https://doi.org/10.4103/2152-7806.82248>
- 650 Chougule, P. S., Najjar, R. P., Finkelstein, M. T., Kandiah, N., & Milea, D. (2019). Light-induced
- 651 pupillary responses in Alzheimer's disease. *Frontiers in Neurology*, 10(APR), 1–12.
- 652 <https://doi.org/10.3389/fneur.2019.00360>
- 653 CIE. (2018). *CIE System for Metrology of Optical Radiation for ipRGC-Influenced Responses to*
- 654 *Light*. CIE Central Bureau.
- 655 Clarke, R. J., Zhang, H., & Gamlin, P. D. R. (2003a). Characteristics of the pupillary light reflex in
- 656 the alert rhesus monkey. *Journal of Neurophysiology*, 89(6), 3179–3189.
- 657 <https://doi.org/10.1152/jn.01131.2002>
- 658 Clarke, R. J., Zhang, H., & Gamlin, P. D. R. (2003b). Primate pupillary light reflex: Receptive field

SYSTEM FOR RESEARCHING THE PUPIL LIGHT REFLEX

31

- 659 characteristics of pretectal luminance neurons. *Journal of Neurophysiology*, 89(6), 3168–3178.
- 660 <https://doi.org/10.1152/jn.01130.2002>
- 661 Cole, B. L., Lian, K. Y., & Lakkis, C. (2006). The new richmond HRR pseudoisochromatic test for
- 662 colour vision is better than the ishihara test. *Clinical and Experimental Optometry*, 89(2), 73–80.
- 663 <https://doi.org/10.1111/j.1444-0938.2006.00015.x>
- 664 Do, M. T. H. (2019). Melanopsin and the intrinsically photosensitive retinal ganglion cells: biophysics
- 665 to behavior. *Neuron*, 104(2), 205–226. <https://doi.org/10.1016/j.neuron.2019.07.016>
- 666 Feigl, B., & Zele, A. J. (2014). Melanopsin-expressing intrinsically photosensitive retinal ganglion
- 667 cells in retinal disease. *Optometry and Vision Science*, 91(8), 894–903.
- 668 <https://doi.org/10.1097/OPX.0000000000000284>
- 669 Girkin, C. A. (2003). Evaluation of the pupillary light response as an objective measure of visual
- 670 function. *Ophthalmology Clinics of North America*, 16(2), 143–153.
- 671 [https://doi.org/10.1016/S0896-1549\(03\)00002-6](https://doi.org/10.1016/S0896-1549(03)00002-6)
- 672 Hall, C. A., & Chilcott, R. P. (2018). Eyeing up the future of the pupillary light reflex in
- 673 neurodiagnostics. *Diagnostics*, 8(1). <https://doi.org/10.3390/diagnostics8010019>
- 674 Hayes, T. R., & Petrov, A. A. (2015). Mapping and correcting the influence of gaze position on pupil
- 675 size measurements. *Behavior Research Methods*. <https://doi.org/10.3758/s13428-015-0588-x>
- 676 Hirata, Y., Yamaji, K., Sakai, H., & Usui, S. (2003). Function of the pupil in vision and information
- 677 capacity of retinal image. *Systems and Computers in Japan*, 34(9), 48–57.
- 678 <https://doi.org/10.1002/scj.10344>
- 679 Joyce, D. S., Feigl, B., Cao, D., & Zele, A. J. (2015). Temporal characteristics of melanopsin inputs to
- 680 the human pupil light reflex. *Vision Research*, 107, 58–66.
- 681 <https://doi.org/10.1016/j.visres.2014.12.001>
- 682 Joyce, D. S., Feigl, B., Kerr, G., Roeder, L., & Zele, A. J. (2018). Melanopsin-mediated pupil function
- 683 is impaired in Parkinson’s disease. *Scientific Reports*, 8(1), 1–9. [https://doi.org/10.1038/s41598-](https://doi.org/10.1038/s41598-018-26078-0)
- 684 [018-26078-0](https://doi.org/10.1038/s41598-018-26078-0)
- 685 Kankipati, L., Girkin, C. A., & Gamlin, P. D. R. (2010). Post-illumination pupil response in subjects
- 686 without ocular disease. *Investigative Ophthalmology and Visual Science*, 51(5), 2764–2769.

SYSTEM FOR RESEARCHING THE PUPIL LIGHT REFLEX

32

- 687 <https://doi.org/10.1167/iovs.09-4717>
- 688 Kankipati, L., Girkin, C. A., & Gamlin, P. D. R. (2011). The post-illumination pupil response is
689 reduced in glaucoma patients. *Investigative Ophthalmology and Visual Science*, 52(5), 2287–
690 2292. <https://doi.org/10.1167/iovs.10-6023>
- 691 Kardon, R. H., Anderson, S. C., Damarjian, T. G., Grace, E. M., Stone, E., & Kawasaki, A. (2009).
692 Chromatic Pupil Responses. Preferential Activation of the Melanopsin-mediated versus Outer
693 Photoreceptor-mediated Pupil Light Reflex. *Ophthalmology*, 116(8), 1564–1573.
694 <https://doi.org/10.1016/j.ophtha.2009.02.007>
- 695 Kassner, M., Patera, W., & Bulling, A. (2014). Pupil: An open source platform for pervasive eye
696 tracking and mobile gaze-based interaction. *UbiComp 2014 - Adjunct Proceedings of the 2014*
697 *ACM International Joint Conference on Pervasive and Ubiquitous Computing*, 1151–1160.
698 <https://doi.org/10.1145/2638728.2641695>
- 699 Kelbsch, C., Strasser, T., Chen, Y., Feigl, B., Gamlin, P. D. R., Kardon, R. H., Peters, T., Roecklein,
700 K. A., Steinhauer, S. R., Szabadi, E., Zele, A. J., Wilhelm, H., & Wilhelm, B. J. (2019).
701 Standards in pupillography. *Frontiers in Neurology*, 10(February).
702 <https://doi.org/10.3389/fneur.2019.00129>
- 703 Kret, M. E., & Sjak-Shie, E. E. (2019). Preprocessing pupil size data: Guidelines and code. *Behavior*
704 *Research Methods*, 51(3), 1336–1342. <https://doi.org/10.3758/s13428-018-1075-y>
- 705 Laughlin, S. B. (1992). Retinal information capacity and the function of the pupil. *Ophthalmic &*
706 *Physiological Optics*, 12(2), 161–164. <https://doi.org/10.1111/j.1475-1313.1992.tb00281.x>
- 707 Lei, S., Goltz, H. C., Chandrakumar, M., & Wong, A. M. F. (2014). Full-field chromatic pupillometry
708 for the assessment of the postillumination pupil response driven by melanopsin-containing
709 retinal ganglion cells. *Investigative Ophthalmology and Visual Science*, 55(7), 4496–4503.
710 <https://doi.org/10.1167/iovs.14-14103>
- 711 Levatin, P. (1959). Pupillary Escape in Disease of the Retina or Optic Nerve. *A.M.A. Archives of*
712 *Ophthalmology*, 62(5), 768–779. <https://doi.org/10.1001/archophth.1959.04220050030005>
- 713 Litvan, I., Saposnik, G., Maurino, J., Gonzalez, L., Saizar, R., Sica, R. E. P., & Bartko, J. J. (2000).
714 Clinical / Scientific Notes Selective sparing of pain pathways in a. *Neurology*, 54(2).

SYSTEM FOR RESEARCHING THE PUPIL LIGHT REFLEX

33

- 715 <https://doi.org/10.1212/WNL.54.2.530>
- 716 Loewenfeld, I. E. (1993). *The pupil: Anatomy, physiology and clinical applications*. Butterworth-
717 Heinemann.
- 718 Mathôt, S. (2017). Safe and sensible baseline correction of pupil-size data. *PeerJ*, April, 1–25.
719 <https://doi.org/doi.org/10.7287/peerj.preprints.2725v1>
- 720 Maynard, M. L., Zele, A. J., & Feigl, B. (2015). Melanopsin-mediated post-illumination pupil
721 response in early age-related macular degeneration. *Investigative Ophthalmology and Visual*
722 *Science*, 56(11), 6906–6913. <https://doi.org/10.1167/iovs.15-17357>
- 723 McDougal, D. H., & Gamlin, P. D. (2015). Autonomic control of the eye. *Comprehensive Physiology*,
724 5(1), 439–473. <https://doi.org/10.1002/cphy.c140014>
- 725 McKinney, W. (2010). Data Structures for Statistical Computing in Python. *Proceedings of the 9th*
726 *Python in Science Conference, 1(Scipy)*, 56–61. <https://doi.org/10.25080/majora-92bf1922-00a>
- 727 Meeker, M., Du, R., Bacchetti, P., Privitera, C. M., Larson, M. D., Holland, M. C., & Manley, G.
728 (2005). Pupil examination: validity and clinical utility of an automated pupillometer. *Journal of*
729 *Neuroscience Nursing*, 37(1), 34-40 7p.
- 730 Mittner, M. (2020). pypillometry: A Python package for pupillometric analyses. *Journal of Open*
731 *Source Software*, 5(51), 2348. <https://doi.org/doi.org/10.21105/joss.02348>
- 732 Park, J. C., Moura, A. L., Raza, A. S., Rhee, D. W., Kardon, R. H., & Hood, D. C. (2011). Toward a
733 clinical protocol for assessing rod, cone, and melanopsin contributions to the human pupil
734 response. *Investigative Ophthalmology and Visual Science*, 52(9), 6624–6635.
735 <https://doi.org/10.1167/iovs.11-7586>
- 736 Poehlmann, A. (2019). *Seabreeze (v1.3.0) [computer software]*.
- 737 Provencio, I., Rodriguez, I. R., Jiang, G., Hayes, W. P., Moreira, E. F., & Rollag, M. D. (2000). A
738 novel human opsin in the inner retina. *Journal of Neuroscience*, 20(2), 600–605.
739 <https://doi.org/10.1523/jneurosci.20-02-00600.2000>
- 740 Romagnoli, M., Stanzani Maserati, M., De Matteis, M., Capellari, S., Carbonelli, M., Amore, G.,
741 Cantalupo, G., Zenesini, C., Liguori, R., Sadun, A. A., Carelli, V., Park, J. C., & La Morgia, C.
742 (2020). Chromatic Pupillometry Findings in Alzheimer’s Disease. *Frontiers in Neuroscience*,

SYSTEM FOR RESEARCHING THE PUPIL LIGHT REFLEX

34

- 743 14(August), 1–10. <https://doi.org/10.3389/fnins.2020.00780>
- 744 Rukmini, A. V., Milea, D., & Gooley, J. J. (2019). Chromatic pupillometry methods for assessing
745 photoreceptor health in retinal and optic nerve diseases. *Frontiers in Neurology*, 10(FEB), 1–20.
746 <https://doi.org/10.3389/fneur.2019.00076>
- 747 Sirois, S., & Brisson, J. (2014). Pupillometry. *Wiley Interdisciplinary Reviews: Cognitive Science*,
748 679–692. <https://doi.org/10.1002/wcs.1323>
- 749 Spitschan, M. (2019). Melanopsin contributions to non-visual and visual function. *Current Opinion in*
750 *Behavioral Sciences*, 30(Figure 1), 67–72. <https://doi.org/10.1016/j.cobeha.2019.06.004>
- 751 Spitschan, M., Jain, S., Brainard, D. H., & Aguirre, G. K. (2014). Opponent melanopsin and S-cone
752 signals in the human pupillary light response. *Proceedings of the National Academy of Sciences*
753 *of the United States of America*, 111(43), 15568–15572.
754 <https://doi.org/10.1073/pnas.1400942111>
- 755 Spitschan, M., & Woelders, T. (2018). The method of silent substitution for examining melanopsin
756 contributions to pupil control. *Frontiers in Neurology*, 9(NOV).
757 <https://doi.org/10.3389/fneur.2018.00941>
- 758 Szabadi, E. (2018). Functional Organization of the Sympathetic Pathways Controlling the Pupil:
759 Light-Inhibited and Light-Stimulated Pathways. *Frontiers in Neurology*, 9(December).
760 <https://doi.org/10.3389/fneur.2018.01069>
- 761 Taylor, W. R., Chen, J. W., Meltzer, H., Gennarelli, T. A., Kelbch, C., Knowlton, S., Richardson, J.,
762 Lutch, M. J., Farin, A., Hulst, K. N., & Marshall, L. F. (2003). Quantitative pupillometry, a new
763 technology: Normative data and preliminary observations in patients with acute head injury -
764 Technical note. *Journal of Neurosurgery*, 98(1 SUPPL.), 205–213.
765 <https://doi.org/10.3171/jns.2003.98.1.0205>
- 766 Thompson, H. S. (1966). Afferent pupillary defects. Pupillary findings associated with defects of the
767 afferent arm of the pupillary light reflex arc. *American Journal of Ophthalmology*, 62(5), 860–
768 873. [https://doi.org/10.1016/0002-9394\(66\)91911-8](https://doi.org/10.1016/0002-9394(66)91911-8)
- 769 Troiani, V. (2020). The future of quantitative pupillometry in health and disease. *Clinical Autonomic*
770 *Research*, 0123456789, 2–3. <https://doi.org/10.1007/s10286-019-00655-3>

SYSTEM FOR RESEARCHING THE PUPIL LIGHT REFLEX

35

- 771 Van Stavern, G. P., Bei, L., Shui, Y. B., Huecker, J., & Gordon, M. (2019). Pupillary light reaction in
772 preclinical Alzheimer's disease subjects compared with normal ageing controls. *British Journal*
773 *of Ophthalmology*, 103(7), 971–975. <https://doi.org/10.1136/bjophthalmol-2018-312425>
- 774 Westheimer, G. (1966). The maxwellian view. *Vision Research*, 6(6), 669–682.
775 [https://doi.org/10.1016/0042-6989\(66\)90078-2](https://doi.org/10.1016/0042-6989(66)90078-2)
- 776 Winn, M. B., Wendt, D., Koelewijn, T., & Kuchinsky, S. E. (2018). Best practices and advice for
777 using pupillometry to measure listening effort: An introduction for those who want to get
778 started. *Trends in Hearing*, 22, 1–32. <https://doi.org/10.1177/2331216518800869>
- 779 Winston, M., Zhou, A., Rand, C. M., Dunne, E. C., Warner, J. J., Volpe, L. J., Pigneri, B. A., Simon,
780 D., Bielawiec, T., Gordon, S. C., Vitez, S. F., Charnay, A., Joza, S., Kelly, K., Panicker, C.,
781 Rizvydeen, S., Niewijk, G., Coleman, C., Scher, B. J., ... Weese-Mayer, D. E. (2019).
782 Pupillometry measures of autonomic nervous system regulation with advancing age in a healthy
783 pediatric cohort. *Clinical Autonomic Research*. <https://doi.org/10.1007/s10286-019-00639-3>
- 784 Woodhouse, J. M., & Campbell, F. W. (1975). The role of the pupil light reflex in aiding adaptation to
785 the dark. *Vision Research*, 15(6), 649–653. [https://doi.org/10.1016/0042-6989\(75\)90279-5](https://doi.org/10.1016/0042-6989(75)90279-5)
- 786